MIXED ELEMENT TYPE UNSTRUCTURED GRID GENERATION AND ITS APPLICATION TO VISCOUS FLOW SIMULATION

Wang Gang, Ye Zheng-yin
College of Aeronautics, Northwestern Polytechnic University, Xi'an, 710072, China

Keywords: *unstructured grid, finite-volume method, Navier-Stokes equations, turbulence model*

Abstract

In this paper, a method is presented for the viscous flow simulations by solving the Navier-Stokes equations on three-dimensional mixed element type unstructured grids. Pirzadeh's advancing-layer method is modified to generate high quality mixed prismatic/pyramid/ tetrahedral element type unstructured grids in boundary-layer region, and advancing-front method is used to construct isotropic tetrahedral grids in the residual flow region. Three-dimensional Navier-Stokes equations are solved by using a cell-centered finite-volume method with AUSM$^+$-up scheme and Spalart-Allmaras one-equation turbulence model. Time is advanced by an implicit Gauss-Seidel relaxation procedure which is constructed by using the first-order linearizing of flux vector and the maximal eigenvalue splitting of flux Jacobian matrix. Adaptive local time stepping and residual averaging are used to accelerate convergence. The assessments of the presented method are derived from the simulation of viscous flow problems around the ONERA M6 wing, DLR-F6 wing-body vs. DLR-F6 wing-body-pylon-nacelle configuration and a business jet configuration.

1 Introduction

Unstructured grid technology is a promising approach offering geometric flexibility for handling of both complex configurations and flows. Compare with the structured grid, the unstructured grid has the merits of excellent flexibility, universal applicability for complex configurations and highly automatic grid generation process. Several unstructured grid generation and flow solver procedures have been developed and successfully demonstrated for inviscid flow around complex configurations. However, for viscous flow simulations, further improvement in efficiency, accuracy and robustness of unstructured grid generation and flow solver procedures are still needed.

Up to now, several kinds of unstructured grid generation strategies for viscous flow applications have been developed such as a hybrid structured/unstructured grids by Soetrisno[1], a advancing-layer method by Pirzadeh[2] and mixed element type unstructured grid generation method by Marcum[3]. All these methods produce semi-structured anisotropic elements adjacent to solid boundaries and use isotropic tetrahedral elements to fill with the outside region. The use of anisotropic prismatic grid in boundary-layer region can reduce the memory and CPU requirement for the flow solver without loss the geometry flexibility and robustness of unstructured grids.

In this paper, a method is presented for the viscous flow simulations by solving the Navier-Stokes equations on three-dimensional mixed element type unstructured grids. Pirzadeh's advancing-layer method is modified to generate high quality mixed prismatic/pyramid/ tetrahedral element type unstructured grids in boundary-layer region, and advancing-front method is used to construct isotropic tetrahedral grids in the residual flow region. Three-dimensional Navier-Stokes equations are solved by using an AUSM$^+$-up [4] type cell-centered finite-volume method and Spalart-Allmaras[5] one-equation turbulence model. The temporal

integration is an implicit Gauss-Seidel relaxation procedure [6] which is based on the first-order linearizing of flux vector and the maximal eigenvalue splitting of flux Jacobian matrix. A new adaptive local time stepping method was developed to eliminate the adverse influence of some poor-quality grids on solve stability and convergence speed. The assessments of these modifications will be derived from the simulation of viscous flow problems around the ONERA M6 wing, DLR-F6 wing-body and DLR-F6 wing-body-pylon-nacelle configuration [7] and a business jet configuration.

2 Numerical Approaches

2.1 Grid Generation

The advancing-layer method has proved very useful when generating the anisotropic tetrahedral grids in viscous region. Here, this method is modified to generate mixed prismatic/pyramid/ tetrahedral element type unstructured grids in boundary-layer region. The mixed element type unstructured grid generation method can be divided into the following steps:

1) Triangulate the solid boundary surface and far field boundary surface. This part of job is similar to the boundary surface grid generation in advancing-front method. The only difference is that the symmetry surface grid needn't to be generated; it will be created automatically after the generation of anisotropic grids in boundary-layer region is finished.

2) Determine a normal vector direction at each solid boundary surface grid point. During the generation of boundary-layer grid, grid points will be distributed along with these normal vectors. A necessary condition to prevent formation of negative volume grid is that the surface vectors at grid points should be visible by all triangular faces connected to the corresponding points. A method is described in Ref.2 for the calculation of normal vector directions on surface grid points.

3) Determine the length of normal vector. According to the predetermined normal vector direction, the process of advancing layers method is performed by successively pushing the layers far away from solid boundary. The advancing of layers will stop if the grid size locally matches the background length or two opposite layers are crossing each other. After the advancing layers stop marching in their locations, the final marching distance between the solid grid points and their corresponding points on current advancing layers is the length of their normal vectors.

4) Generate mixed anisotropic element type unstructured grid. Considering a triangular surface on solid boundary with three grid points 1-2-3 and their corresponding normal vectors (see Fig 1.a), the end points of these normal vectors are labeled as 1′-2′-3′. A prismatic cell can be formed by connecting the above six points. Subsequently, this prismatic cell will be cut into several layers along with boundary normal vectors (see Fig 1.b). The normal grid spacing along the surfaces vector at each layer-cutting process is determined by the following stretching function

$$\delta_n = \delta_0[1 + r_1(1 + r_2)^{n-1}]^{n-1} \qquad (1)$$

here, δ_n is the normal spacing for the nth layer, δ_0 is a prescribed first layer spacing, and the factors r_1, r_2 are constants that determine the rate of stretching.

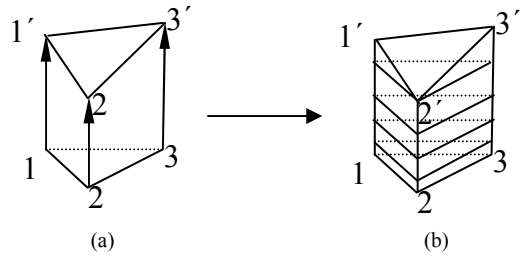

Fig.1. sketch map for the creation of mixed element type unstructured gird

In case of some complex configurations, the length of boundary normal vectors may different from each other. So three possible types of grids, which are prismatic grid,

pyramid grids and tetrahedral grids, are likely to be generated by the last layer-cutting operation. As shown in Fig 1.b, some prismatic grids and a pyramid grid are generated by cutting prismatic cell 1- 2 -3 - 1′-2′-3′ into several layers. After the above cutting operation has carried out on every solid boundary grid surface, the 'viscous' portion of mixed element type unstructured grids is formed.

5) The rest part of the flow domain is filled with isotropic tetrahedral grids by advancing-front method. When the step 4) is finished, the process automatically generates the symmetry surface grid and switches to the conventional advancing-front method to form regular isotropic tetrahedral cells in the rest part of the domain.

2.2 Governing Equations

The fluid motion is governed by the time dependent Navier-Stokes equations for an ideal gas which express the conservation of mass, momentum, and energy for a compressible fluid in the absence of external forces. The equations are given below in integral form for a bounded domain Ω with a boundary $\partial\Omega$

$$\frac{\partial}{\partial t}\iiint_{\Omega} \boldsymbol{Q}\,dV + \iint_{\partial\Omega} \boldsymbol{F}(\boldsymbol{Q})\cdot\boldsymbol{n}\,dS = \iint_{\partial\Omega} \boldsymbol{G}(\boldsymbol{Q})\cdot\boldsymbol{n}\,dS \quad (2)$$

where $\boldsymbol{Q} = \{\rho, \rho u, \rho v, \rho w, e_0\}^T$;

$\boldsymbol{F}(\boldsymbol{Q})\cdot\boldsymbol{n} = (\boldsymbol{V}\cdot\boldsymbol{n})\{\rho, \rho u, \rho v, \rho w, e_0 + p\}^T + p\{0, n_x, n_y, n_z, 0\}^T$;

$\boldsymbol{G}(\boldsymbol{Q})\cdot\boldsymbol{n}$ are viscous fluxes terms.

For idea gas

$$p = (\gamma - 1)(e_0 - \frac{1}{2}\rho(u^2 + v^2 + w^2)),\ h_t = \frac{e_0 + p}{\rho}$$

Here ρ, u, v, w, p, e_0 and h_t are respectively represent density of fluid, velocity components in the x, y and z directions, pressure, total energy of per unit volume and total enthalpy. n_x, n_y, n_z are the Cartesian components of the exterior surface unit normal $\boldsymbol{n}$ on the boundary $\partial\Omega$. γ is the ratio of specific heats and is prescribed as 1.4 for air. For laminar viscous flow, viscosity μ is computed by Sutherland's law.

2.3 Spatial discretization

In order to fit with different grid type, the cell-centered finite-volume spatial discretization is used. On an arbitrary selected grid surface $\boldsymbol{S}_k$, the inviscid flux $\boldsymbol{F}(\boldsymbol{Q}_k)\cdot\boldsymbol{S}_k$ is computed by the AUSM$^+$-up scheme:

$$\boldsymbol{F}(\boldsymbol{Q}_k)\cdot\boldsymbol{S}_k = |\boldsymbol{S}_k| a_k [M_k^+ \{\rho, \rho u, \rho v, \rho w, \rho H_t\}_{kL}^T + M_k^- \{\rho, \rho u, \rho v, \rho w, \rho H_t\}_{kR}^T] + \{0, S_x p_k, S_y p_k, S_z p_k, 0\}^T$$

In this scheme, the conservation variables $\boldsymbol{Q}_{kL}$ and $\boldsymbol{Q}_{kR}$ which are interpolated from the lift and right cells of grid surface $\boldsymbol{S}_k$ should be used. Here, we show the interpolation method of $\boldsymbol{Q}_{kL}$ on different types of cells as an example. Consider three types of grid in Fig.2, number 1, 2, 3, 4, 5, 6 denote the grid vertexes and the letter c stands for the cell center.

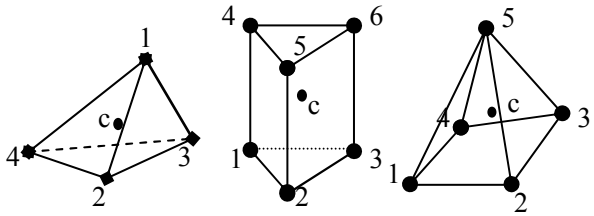

Fig.2. Different types of grid element

For the tetrahedral cell showed in Fig.2 (a), we assume that the grid surface $\boldsymbol{S}_k$ is constituted by vertex 2, 3 and 4. Then the $\boldsymbol{Q}_{kL}$ can be calculated with the following expression

$$\boldsymbol{Q}_{kL} = \boldsymbol{Q}_c + [(\boldsymbol{Q}_2 + \boldsymbol{Q}_3 + \boldsymbol{Q}_4)/3 - \boldsymbol{Q}_1]/4 \quad (4)$$

For the prismatic cell showed in Fig.2 (b), if grid surface $\boldsymbol{S}_k$ is a downside triangle constituted by vertex 1,2 and 3, then the $\boldsymbol{Q}_{kL}$ can be interpolated by using the following expression

$$\boldsymbol{Q}_{kL}=\boldsymbol{Q}_c+(\boldsymbol{Q}_1+\boldsymbol{Q}_2+\boldsymbol{Q}_3)/6-(\boldsymbol{Q}_4+\boldsymbol{Q}_5+\boldsymbol{Q}_6)/6 \quad (5)$$

If grid surface $\boldsymbol{S}_k$ is a side quadrangle face constituted by vertex 1, 2, 4 and 5, then the $\boldsymbol{Q}_{kL}$ can be interpolated by using the following expression

$$\boldsymbol{Q}_{kL}=\boldsymbol{Q}_c+(\boldsymbol{Q}_1+\boldsymbol{Q}_2+\boldsymbol{Q}_4+\boldsymbol{Q}_5)/12-(\boldsymbol{Q}_3+\boldsymbol{Q}_6)/6 \quad (6)$$

For the pyramid grid showed in Fig.2 (c), if grid surface $\boldsymbol{S}_k$ is a downside quadrangle face constituted by vertex 1, 2, 3 and 4, then the $\boldsymbol{Q}_{kL}$ can be calculated with the following expression

$$\boldsymbol{Q}_{kL}=\boldsymbol{Q}_c+[(\boldsymbol{Q}_1+\boldsymbol{Q}_2+\boldsymbol{Q}_3+\boldsymbol{Q}_4)/4-\boldsymbol{Q}_5]/5 \quad (7)$$

If $\boldsymbol{S}_k$ is a side triangle face, we can assume that it is constituted by vertex 1, 2 and 5, then $\boldsymbol{Q}_{kL}$ can be interpolated by using the following expression

$$\boldsymbol{Q}_{kL}=\boldsymbol{Q}_c+[(\boldsymbol{Q}_1+\boldsymbol{Q}_2+\boldsymbol{Q}_5)/3-(\boldsymbol{Q}_3+\boldsymbol{Q}_4)/2]/4 \quad (8)$$

The essential solution vectors on cell centers and vertexes will be both needed when using the formula (4) ~ (8) to calculate essential solution vectors on grid surface. But for cell-centered finite-volume scheme the essential solution vectors on grid vertexes cannot be achieved directly, thus a reconstruction process should be employed. The details of the reconstruction method have been introduced in Ref.8.

The viscous flux $\boldsymbol{R}_1=\sum_{All\ faces}\boldsymbol{G}(\boldsymbol{Q})\cdot\boldsymbol{n}\Delta S$ is computed by standard central difference scheme. When finite volume method is applied on each grid cell, we can get a set of semi-discrete form equations

$$V_i\frac{\mathrm{d}\boldsymbol{Q}}{\mathrm{d}t}+\sum_{All\ faces}\boldsymbol{F}(\boldsymbol{Q})\cdot\boldsymbol{n}\Delta S=\boldsymbol{R}_1,\quad i=1,2,3.....N \quad (9)$$

2.4 Implicit time integration

Based on the first-order linearizing the inviscid flux term of equation (9) and the assumption of treating the viscous flux term explicitly, equation (9) can be expressed in the flowing style

$$V_i\frac{\Delta\boldsymbol{Q}_{ic}}{\mathrm{d}t}+\sum_{All\ faces}\boldsymbol{A}\Delta\boldsymbol{Q}=-\sum_{All\ faces}\boldsymbol{F}(\boldsymbol{Q}^n)\cdot\boldsymbol{n}\Delta S+\boldsymbol{R}_1(\boldsymbol{Q}^n) \quad (10)$$

where, $\Delta\boldsymbol{Q}=\boldsymbol{Q}^{n+1}-\boldsymbol{Q}^n$,subscript *ic* denotes to the values of $\Delta\boldsymbol{Q}$ at the center of cell *i*. The flux Jacobian matrix $\boldsymbol{A}$ has real eigenvalues and may be split into two matrices by using the maximal eigenvalue splitting technology,

$$\boldsymbol{A}^+=\frac{\boldsymbol{A}+\boldsymbol{I}\beta\lambda_{\max}}{2};\quad \boldsymbol{A}^-=\frac{\boldsymbol{A}-\boldsymbol{I}\beta\lambda_{\max}}{2} \quad (11)$$

According to the direction of propagation of information in the flow, $\boldsymbol{A}\Delta\boldsymbol{Q}$ can be approximated as $\boldsymbol{A}^+\Delta\boldsymbol{Q}_{ic}+\boldsymbol{A}^-\Delta\boldsymbol{Q}_{neighbor}$, Then equation (10) becomes

$$[\frac{V_i}{\Delta t}\boldsymbol{I}+\sum_{Allfaces}\boldsymbol{A}^+]\Delta\boldsymbol{Q}_{ic}=\boldsymbol{R}_1(\boldsymbol{Q}^n)-\sum_{Allfaces}\boldsymbol{F}(\boldsymbol{Q}^n)\cdot\boldsymbol{n}\Delta S-\sum_{Allfaces}\boldsymbol{A}^-\Delta\boldsymbol{Q}_{neighbc} \quad (12)$$

A Gauss-Seidel relaxation approach is used to solve the equation (12). For steady case, time accuracy in the integration is not required, so the solution convergence to steady can be accelerated by implicit residual smoothing and local time stepping. For mixed element type unstructured grid, the following local time stepping form is usually adopted

$$\Delta t_i=\frac{CFL}{m}\sum_{k=1}^{m}\frac{V_i}{\left|uS_x+vS_y+wS_z\right|+a_i\sqrt{(S_x^2+S_y^2+S_z^2)}} \quad (13)$$

Here V_i is the volume of grid cell i, *CFL* is the CFL number, S_x, S_y and S_z are the projected areas of each grid surface in x, y and z directions, a_i is the local speed of sound and *m* is the surface number of cell i.

Numerical experiments indicate that some poor-quality grids will remarkably influence the stability and convergence speed, when equation (13) is used to evaluate the local time steps. The main cause for this is that the local steps decided by equation (13) will exceed stability

limit on the time step for those poor-quality grids, but for those good-quality grids equation (13) is too conservative. Generally speaking, there are only very few poor-quality cells among the total tetrahedral grids. So in order to eliminate the adverse influence of some poor-quality grids on solve stability and convergence speed, we developed the following modified equation for computing local time steps

$$\Delta t_i = \frac{CFL}{m}(\alpha+\beta_i)\sum_{k=1}^{m}\frac{V_i}{|uS_x+vS_y+wS_z|+a_i\sqrt{(S_x^2+S_y^2+S_z^2)}} \quad (14)$$

In this formula, β_i is the quality factor of grid cell i. For tetrahedral cells, the range of β_i is from 0.0 to 1.0 according to the definition of Ref.9. Tetrahedral cells with quality factor near 1.0 are nearly equilateral while those tetrahedral cells with low quality factor look like thin slices. For the other two types of cells, β_i is the ratio of the shortest edge length to the longest edge length of grid cell i. α is an empirically-chosen coefficient, its recommended value is a number between 0.3 and 0.5.

2.5 Turbulence model

For the current study, closure of the Reynolds stress is provided by Spalart-Allmaras one-equation turbulence model. This model is based on a transport equation written for a variable $\hat{\upsilon}$ linked to the eddy viscosity by:

$$\mu_T = \rho\hat{\upsilon}f_{v1};\ f_{v1}=\frac{\chi^3}{\chi^3+C_{v1}^3};\ \chi=\frac{\hat{\upsilon}}{\upsilon};\ C_{v1}=7.1 \quad (15)$$

the transport equation related to the dependent variable $\hat{\upsilon}$ is written as

$$\frac{D\hat{\upsilon}}{Dt}=C_{b1}[1-f_{t2}]\hat{S}\hat{\upsilon}+\frac{1}{\sigma}[\nabla\cdot((\upsilon+\hat{\upsilon})\nabla\hat{\upsilon})+C_{b2}(\nabla\hat{\upsilon})^2] - [C_{w1}f_w-\frac{C_{b1}}{\kappa^2}f_{t2}][\frac{\hat{\upsilon}}{d}]^2+f_{t1}\Delta U^2 \quad (16)$$

The above equation is solved by using the cell-centered finite-volume spatial discretization and backward-Euler time-stepping-scheme.

3 Results

Three test cases are presented in this section to show the practicability, accuracy and robustness of the mixed element type unstructured grid generation and the viscous flow simulation method. During the grid generation process, uniform first layer spacing $\delta_0 = 2.0\times10^{-5}$ is prescribed, and the factors r_1, r_2 are set to 0.1 and 0.15.

3.1 ONERA M6 Wing

For the ONERA M6 wing configuration, the viscous flow simulation is performed at the flow condition of Re=1.17×10^7, M_∞=0.84, α=5.06°, which represent a high-Reynolds-number, transonic, separated flow condition. The surface grid on solid and symmetry boundary is shown in Fig 3. Fig 4 shows the velocity profile of boundary layer on the symmetry surface.

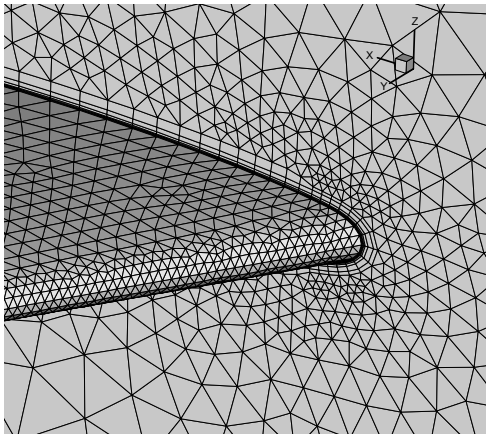

Fig.3. The solid and symmetry boundary surface grid

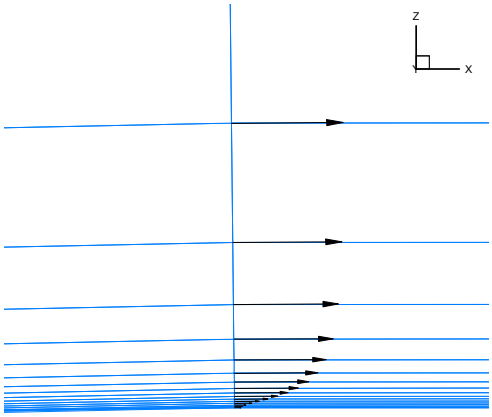

Fig.4. Velocity profile of boundary layer on the symmetry surface

In Fig. 5 shows the chord-wise *Cp* distribution at η=0.80 and η=0.90 chord stations. By comparing the *Cp* distribution in Fig.5 with the experimental data, we can easily draw the conclusion that the viscous flow solver of this paper has good ability for simulating the shock induced separation on the outboard portion of the wing.

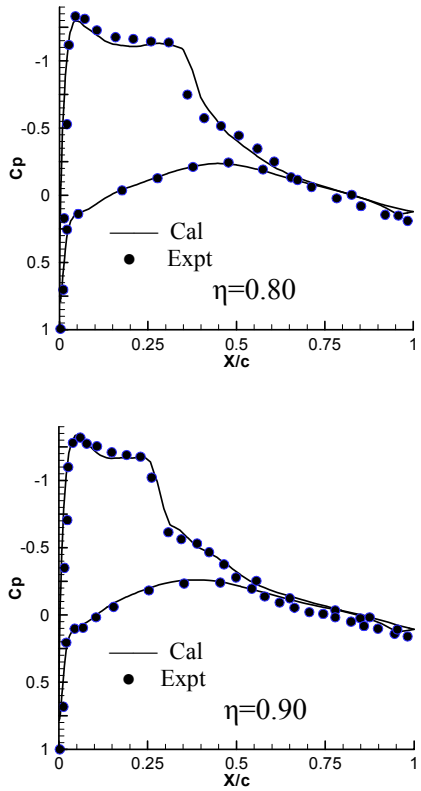

Fig. 5. The chord-wise Cp distribution of M6 wing

3.2 DLR-F6 wing-body and DLR-F6 wing-body-pylon-nacelle configuration

For the DLR-F6 wing-body and DLR-F6 wing-body-pylon-nacelle configuration, the viscous flow simulation is performed at the flow condition of $Re=3.0\times10^6$, $M_\infty=0.75$, $\alpha=1.0^\circ$. The surface grid on solid and symmetry boundary is shown in Fig. 6 and Fig. 7. Fig.8 present the surface pressure coefficient *Cp* distribution of the above two wing-body configurations at the pylon inboard (η=0.331) and outboard (η=0.377) chord-wise stations. In Fig. 8, we can find that the pylon and nacelle have severe influence on the pressure distribution of wing, which will result in a lift loss accompanying with the increasing of drag. The computed results agree well with the experimental data, this shows that the method of this paper has excellent accuracy in predicting the aerodynamic influence of the pylon and nacelle. In Fig. 9, the comparison of the calculated streamlines at the wing-body junction with the experimental oil flow is presented. This figure clearly indicates that the bubble area at the tailing edge of wing-body junction can be well simulated.

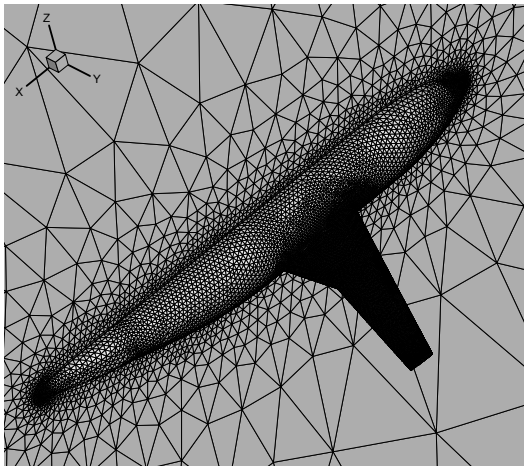

Fig. 6. Surface grid on solid and symmetry boundary of DLR-F6 wing-body configuration

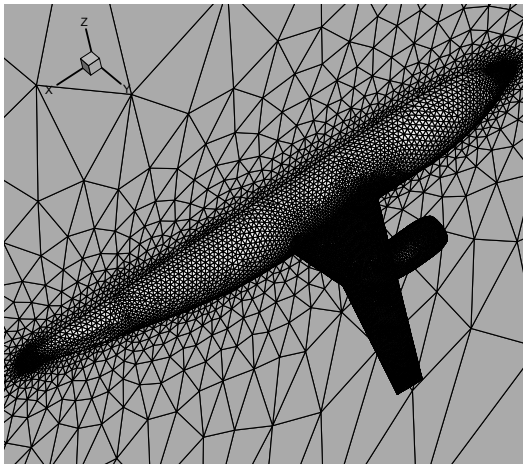

Fig. 7. Surface grid on solid and symmetry boundary of DLR-F6 wing-body-pylon-nacelle configuration

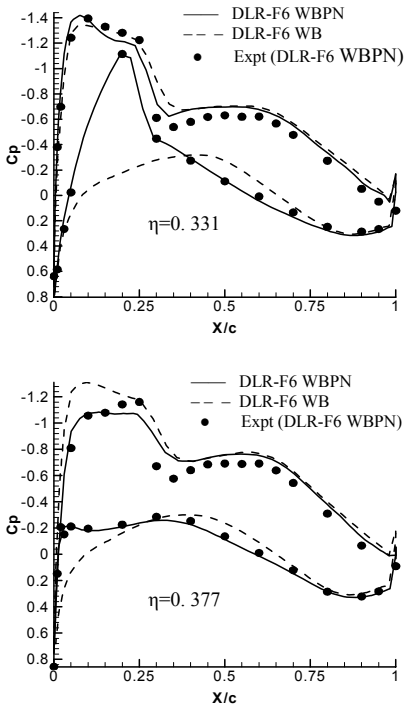

Fig. 8. The chord-wise Cp distribution of DLR-F6 wing-body and DLR-F6 wing-body-pylon-nacelle configuration

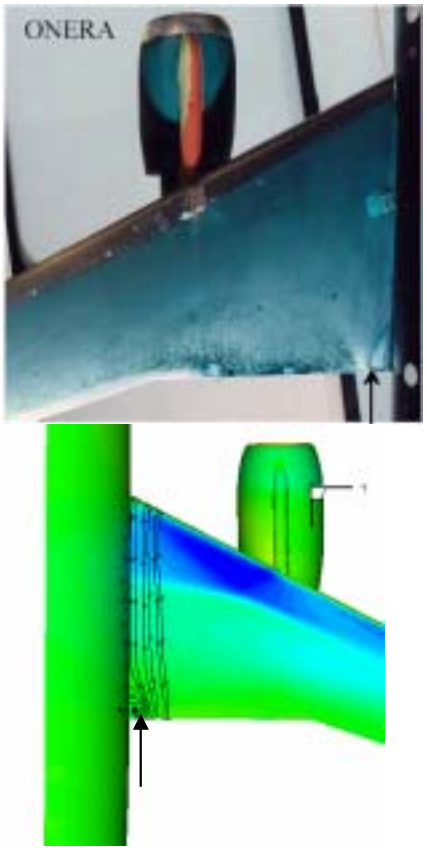

Fig. 9. Comparison of the calculated streamlines (bubble area) at the wing-body junction with the experimental oil flow

3.3 A business jet

Finally, as an example of application, the developed method has been used to compute the transonic flow around a business jet configuration. The boundary grid used in the computation is shown in Fig. 10. The computation is performed at a Mach number of 0.8, a Reynolds number of 3 million, and an angle of attack of 1.8°. The computed pressure coefficient contours on the surface of the business jet and symmetry boundary are displayed in Fig. 11. In Fig. 11, we can find that the postpositive engine has significant influence about the distribution of the pressure on the up-wing and after-body surface.

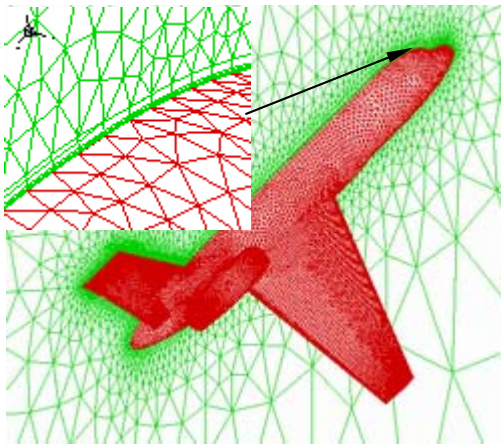

Fig. 10. Boundary grid of business jet configuration

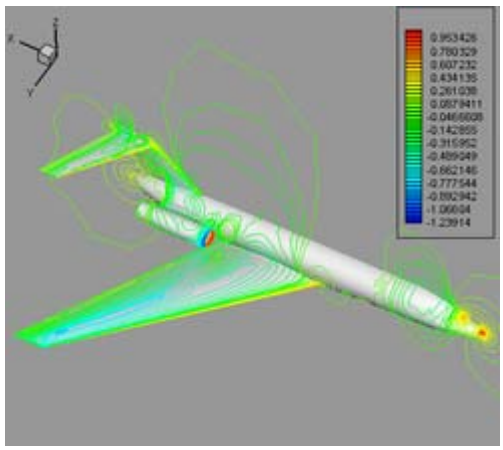

Fig. 11. Pressure coefficient contours on the surface of the business jet and symmetry boundary

4 Conclusions

A method for the mixed element type unstructured viscous grid generation has been introduced. Three-dimensional Navier-Stokes equations are solved by using a cell-centered finite-volume method with AUSM^{+}-up scheme and Spalart-Allmaras one-equation turbulence model. Time is advanced by an implicit Gauss-Seidel relaxation procedure which is constructed by using the first-order linearizing of flux vector and the maximal eigenvalue splitting of flux Jacobian matrix. A new local time stepping method was developed to eliminate the adverse influence of some poor-quality grids on solve stability and convergence speed. The simulation of three typical viscous flow problems show that the grid generation and numerical solution method has the merits of practicability, accuracy and robustness, so it is particularly useful in handling viscous flow problems around complex configurations with unstructured grid methodology.

References

[1] Soetrisno M, Imlay S T, Roberts D W and Taflin D E. Computation of Viscous Flows for Multi-Element Wings Using Hybrid structured-Unstructured Grids, AIAA Paper 97-0623, 1997.

[2] Pirzadeh S. Three-Dimensional Unstructured Viscous Grids by the Advancing-Layer Method. *AIAA Journal*, Vol. 34, No.1, pp 43～49, 1996.

[3] Marcum D L, Gaither J A. Mixed Element Type Unstructured Grid Generation for Viscous Flow Applications, AIAA Paper 99-3252, 1999.

[4] Liou M S. A Further Development of the AUSM+ Scheme towards Robust and Accurate Solutions for All Speeds, AIAA Paper 2003-4116, 2003.

[5] Spalart P, Allmaras S. A one-equation turbulence model for aerodynamic flows, AIAA Paper 92-0439, 1992.

[6] Tomaro R F, Strang W Z and Sankar L N. An Implicit Algorithm for Solving Time Dependent Flows on Unstructured Grids, AIAA Paper 97-0333, 1997.

[7] Brodersen O, Sturmer A. Drag Prediction of Engine-Airframe Interference Effects Using Unstructured Navier-Stokes Calculations, AIAA Paper 2001-2414, 2001

[8] Frink N T. Assessment of an unstructured-grid method for predicting 3-D turbulent viscous flows. AIAA Paper 96-0292, 1996.

[9] Golias N A, Tsiboukis T D. An Approach to Refining Three Dimensional Tetrahedral Meshes based on Delaunay Transformations. *Int J Num Meth Eng*, Vol. 37, No. 5, pp 793～812, 1994.